Original Article

Journal of Intelligent Material Systems and Structures

Journal of Intelligent Material Systems and Structures
2014, Vol. 25(15) 1965–1977

DOI: 10.1177/1045389X13512906
jim.sagepub.com
SAGE

Design of a robust quantitative feedback theory position controller for an ionic polymer metal composite actuator using an analytical dynamic model

Hossein Moeinkhah, Alireza Akbarzadeh and Jalil Rezaeepazhand

Abstract

Nowadays, ionic polymer metal composite actuators are widely used in many fields such as biometric, biomedical, and micro-manipulator devices. Although extensive research exists on control of the ionic polymer metal composite actuators, not much research has been done on robust control considering the nonlinear dynamics of the ionic polymer metal composite. In this study, for the first time, a closed-loop robust controller based on quantitative feedback theory is designed to overcome the actuation performance degradation of the ionic polymer metal composite actuators. First, an analytical electromechanical model is developed to fully describe dynamics of the flexible ionic polymer metal composite actuator. The model is based on the Euler–Bernoulli beam theory and includes structural damping to model viscoelastic behavior of the ionic polymer metal composite actuator. Considering the highly nonlinear and uncertain dynamics of the ionic polymer metal composite actuator, a feedback controller based on quantitative feedback theory is designed to suppress the arbitrary external disturbances and consistently track desired input. Results indicate that the robust quantitative feedback theory control techniques can significantly improve the ionic polymer metal composite performance against nonlinearity and parametric uncertainties.

Keywords

Ionic polymer metal composite, robust control, quantitative feedback theory, Golubev method

Introduction

Recently, the trend of new actuator applications has led researchers to develop novel actuation materials which are light, compact, and driven by low power. Electroactive polymers (EAPs) are emerging as a new class of actuation materials. These actuators have been extensively studied because of their potential applications in robotics, biomedical devices, and artificial muscles (Bar-Cohen and Zhang, 2008; Jo et al., 2013). Ionic polymer metal composites (IPMCs) are a class of EAPs and are good candidates for biomimetic sensors and actuators (Shahinpoor and Kim, 2001). In comparison with traditional hydraulic or electric actuators, IPMC actuators offer several advantages such as low driving voltage, large stroke, low power consumption, and potential use in biomimetic applications.

A typical IPMC actuator is composed of a soft ionic polymer membrane and two thin metallic electrode layers. Applying voltage, across the conductive electrodes, causes migration of the cations and water molecules to cathode side. This mechanism leads to bending of the IPMC and hence the actuation effect (Kim and Shahinpoor, 2003). These novel materials have a wide range of applications, including bio and micromanipulation systems (McDaid et al., 2010; Panda and Dutta, 2010; Santos et al., 2010), biomimetic robots (Guo et al., 2003; Jeon et al., 2009; Jung et al., 2010; Kim et al., 2003; Yamakita et al., 2005; Yeom and Oh, 2009), and industrial and biomedical devices (Feng and Tsai, 2011; Shahinpoor and Kim, 2005; Yousef et al., 2011).

A good understanding of system dynamics is crucial to successful control application of an IPMC actuator.

Department of Mechanical Engineering, Center of Excellence on Soft Computing and Intelligent Information Processing (SCIIP), Ferdowsi University of Mashhad, Mashhad, Iran

Corresponding author:
Hossein Moeinkhah, Department of Mechanical Engineering, Center of Excellence on Soft Computing and Intelligent Information Processing (SCIIP), Ferdowsi University of Mashhad, P.O. Box: 91775-1119, Mashhad 9177948944, Iran.
Email: hmoein@gmail.com

Several dynamic models have been proposed for predicting the behavior and performance of the IPMC actuators. They may be classified into three categories, namely, the black box model (Kanno et al., 1996), gray box model (Bonomo et al., 2007; Newbury and Leo, 2003), and physical model (Branco and Dente, 2006; Chen et al., 2007, 2010, 2013; Nemat-Nasser and Li, 2000; Porfiri, 2009; Pugal et al., 2011; Yim et al., 2007). Thus far, the physical models which attempt to explain the underlying physics of sensing and actuation responses of the IPMCs are more accurate than the other models. Chen et al. (2010) reported modeling of a robotic fish propelled by an IPMC actuator and considered the interactions between IPMC and fluid. Yim et al. (2007) proposed a finite element method for modeling the motion of an IPMC actuator underwater. They used an empirical resistance–capacitance (RC) circuit to predict the bending moment of an IPMC under electrical stimuli. In our previous studies, an exact electromechanical model was developed to fully describe dynamics of the IPMC actuators with structural damping, hydrodynamic loading, and electromechanical force (Moeinkhah et al., 2013a, 2013b). In this study, to better explain the highly nonlinear dynamic responses of the IPMC actuators, an analytical dynamic model incorporating the effects of both electrical and mechanical responses is developed. The proposed electromechanical model consists of an electrical impedance model based on a distributed RC line and a mechanical dynamic model. The mechanical dynamic model is based on the Euler–Bernoulli beam theory and structural damping to model viscoelastic behavior of the IPMC actuator.

In spite of the positive characteristics of the IPMC actuators, they have some disadvantages such as hysteresis, back relaxation, low blocking force, and highly uncertain and nonlinear dynamics (Bar-Cohen, 2004; Kim, 2007; Kim and Kim, 2007; Takagi et al., 2012). These features may lead to oscillation and instability in the system performances. To overcome these problems, some control methods are proposed for the IPMC actuators. The simplest control method that can be used for the IPMC actuators is open-loop activation. Open-loop position response of an IPMC is not repeatable (Bhat and Kim, 2004b). Additionally, it is difficult to keep its tip displacement at a desired position (Bhat and Kim, 2003; Richardson et al., 2003). Hence, the closed-loop precision control scheme should be applied to ensure proper functioning, repeatability, and reliability. For example, a lead-lag compensator, as a linear control scheme, was implemented for position and force control of an IPMC actuator based on hybrid control strategy (Bhat and Kim, 2004a). Other conventional linear control methodologies such as the linear quadratic regulator (LQR) controller (Mallavarapu and Leo, 2001), proportional–integral–derivative (PID) controller (Bandopadhya et al., 2008; Yun and Kim, 2006) have been applied to improve the actuator response. However, the nonlinear and time-variant behavior of the IPMCs degrades the performance of linear controllers (Liu et al., 2011). It is shown (Kang et al., 2007) that for the IPMC actuators, robust control techniques achieve better controlling performance over the conventional controllers. Therefore, to overcome the highly nonlinear and uncertain dynamics of the IPMC actuators, a number of control schemes such as robust control using H_∞ controllers (Chen and Tan, 2008), model reference adaptive control (MRAC) (Brufau-Penella et al., 2008; La and Sheng, 2009; Lavu et al., 2005), and fuzzy logic control (Khadivi et al., 2007; Thinh et al., 2009) are implemented. Recently, Ahn et al. (2010) applied quantitative feedback theory (QFT) for position control of the IPMC actuators using a second-order empirical model of the plant. However, this model does not predict the highly nonlinear behavior of the IPMC actuator due to limitation of its second-order model. To the best of our knowledge, their study is the only available work on the robust control of IPMC actuators using QFT techniques. Moreover, a theoretical model based on QFT controller for precision control of an IPMC actuator has not yet been presented. In this article, considering the nonlinear dynamics of the IPMC actuator, a feedback controller based on QFT is demonstrated which is robust against the plant nonlinearities and uncertainties.

The remaining of this article is organized as follows: In section "Actuator dynamic model," dynamic model of the IPMC is derived. First, the electrical impedance model of the actuator is obtained based on a distributed RC line theory. Then, the obtained infinite-dimensional model is reduced to a family of third-order system using Golubev method (Golubev and Horowitz, 1982). To carefully explain the highly nonlinear dynamic responses of the IPMC actuator, the electromechanical dynamic model is obtained based on Euler–Bernoulli beam theory. The exact mechanical dynamic model is derived by considering structural damping and hydrodynamic loading effects. Next, the infinite-dimensional dynamics model is replaced with a family of fourth-order linear uncertain transfer functions based on Golubev method. In section "QFT control strategy," a robust controller based on QFT is designed for robust stability, tracking, and disturbance rejection problems. In section "Simulation of design," robustness of the proposed controller is demonstrated and comparison with a PID controller is presented using several simulations. Finally, in section "Conclusion," concluding remarks are made.

Actuator dynamic model

The complete dynamic model of the actuator is composed of two parts, namely, an electrical model and an electromechanical model. The electrical model is related

to the input voltage and ion movement inside the IPMC actuator, while the electromechanical model describes the relation between input voltage and bending displacement of the actuator.

Electrical impedance model

Many researchers have modeled the actuation of the IPMCs using electrical circuits (Kanno et al., 1996; Newbury and Leo, 2003). Bao et al. (2002) showed that the lumped RC model could not fit the time response between the experimental and simulated data for an IPMC sample. The variation in the capacitance values in the IPMC, produced by dendrite structure of electrodes, is the main source of this discrepancy. Kanno et al. (1996) incorporated this effect and proposed a distributed model for an IPMC strip. They divided an IPMC strip into 10 segments consisting of RC circuits and modeled the relation between the input current and tip displacement. Another similar distributed equivalent circuit is described by Shahinpoor and Kim (2000) which consists of four elements in each single unit. In our previous study, a distributed electrical circuit was presented for deriving a mathematical expression for the electrical impedance of an IPMC actuator. An infinite-dimensional impedance model was developed and next replaced with a simple second-order model using Golubev method (Moeinkhah et al., 2013b).

In this study, to better investigate the electrical behavior at the interface between the polymer and the metal electrodes, the original distributed RC model introduced in Moeinkhah et al. (2013b) is further improved (see Figure 1). Figure 1 illustrates the improved distributed RC model of the IPMC actuator. In this model, R_s is the surface resistance and the branches C_1–R_1 and C_2–R_2 represent the electrical behavior at the interface of metal and polymer in the upper and lower surfaces, respectively. The electrolyte between the electrodes introduces an internal resistance, which is represented by R_P as a shunt resistor between two electrodes in a single unit.

As a first step in deriving the actuation model of an IPMC actuator, we will develop the electrical impedance model. For simplicity, we transfer the single-unit circuit shown in Figure 1 into an equivalent circuit as shown in Figure 2.

Let $Z_1(s)$ and $Z_2(s)$ be series and parallel impedance, respectively, which can be defined as

$$Z_1(s) = 2R_s \tag{1}$$

$$Z_2(s) = \frac{R_P(1 + RCs)}{(R_P + R)Cs + 1} \tag{2}$$

where $R = R_1 + R_2$ and $1/C = (1/C_1) + (1/C_2)$.

By applying Kirchhoff's law to the infinitesimal element, Δx, the following current and voltage relations can be written in Laplace domain

$$\frac{\partial v(x,s)}{\partial x} + Z_1(s)i(x,s) = 0 \tag{3}$$

$$\frac{\partial i(x,s)}{\partial x} + \frac{v(x,s)}{Z_2(s)} = 0 \tag{4}$$

By substituting $i(x, s)$ from equation (3) into equation (4), one can obtain the following partial differential equation (PDE)

$$\frac{\partial^2 v(x,s)}{\partial x^2} - \frac{Z_1(s)}{Z_2(s)}v(x,s) = 0 \tag{5}$$

Considering the following boundary conditions for voltage and current

$$\begin{aligned} v(0,s) = V_0(s),\ \ i(0,s) = I_0(s),\ \ i(L,s) \\ = -\frac{1}{Z_1(s)}\frac{\partial v(x,s)}{\partial x}\bigg|_{x=L} = 0 \end{aligned} \tag{6}$$

the solution for equation (5) can be obtained as

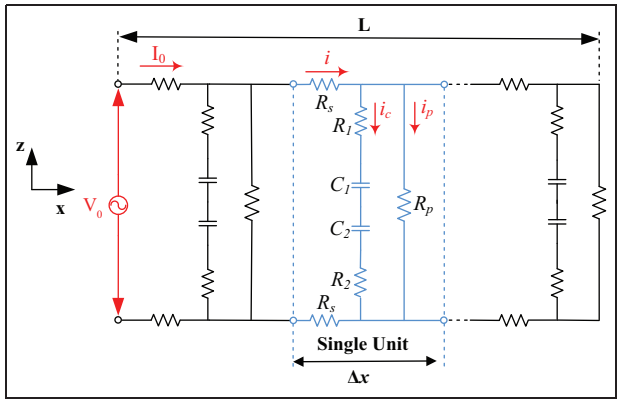

Figure 1. Distributed RC model of an IPMC actuator.
RC: resistance–capacitance; IPMC: ionic polymer metal composite.

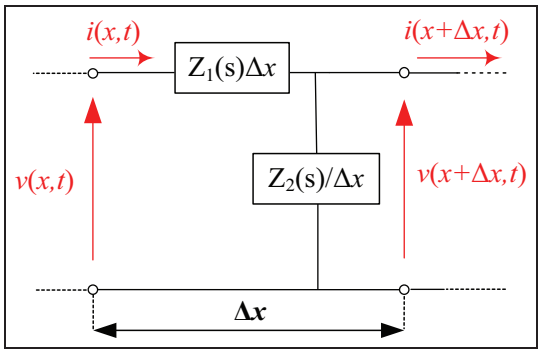

Figure 2. Equivalent single-unit circuit.

Table 1. Values of identified parameters for impedance.

Parameters	R_s (Ω cm^{-1})	R_1 (Ω cm)	R_2 (Ω cm)	R_p (Ω cm)	C_1 (F cm^{-1})	C_2 (F cm^{-1})
Identified value	35.34	15.734	13.253	3.465e4	0.01573	0.0176

$$v(x,s) = V_0(s)\left(\cosh\left(\sqrt{\frac{Z_1(s)}{Z_2(s)}}x\right) - \tanh\left(\sqrt{\frac{Z_1(s)}{Z_2(s)}}L\right)\sinh\left(\sqrt{\frac{Z_1(s)}{Z_2(s)}}L\right)\right) \quad (7)$$

Substituting equation (7) into equation (3), the surface current $i(x, s)$ is obtained as

$$i(x,s) = \frac{V_0(s)}{\sqrt{Z_1(s)Z_2(s)}}\left(\tanh\left(\sqrt{\frac{Z_1(s)}{Z_2(s)}}L\right)\cosh\left(\sqrt{\frac{Z_1(s)}{Z_2(s)}}x\right) - \sinh\left(\sqrt{\frac{Z_1(s)}{Z_2(s)}}x\right)\right) \quad (8)$$

Using the initial condition for current at $x = 0$, $i(0, s) = I_0(s)$, the impedance model, $Z(s)$, is

$$Z(s) = \frac{V_0(s)}{I_0(s)} = \frac{\sqrt{Z_1(s)Z_2(s)}}{\tanh\left(\sqrt{\frac{Z_1(s)}{Z_2(s)}}L\right)} \quad (9)$$

Because of the term "tanh" in equation (9), the driven impedance model is infinite-dimensional and not suitable for real-time control of the actuator. Therefore, Golubev method is used to build a suitable model for control of the actuator. By replacing the term "tanh" with its equivalent series in equation (9), the impedance model is obtained as follows

$$Z(s) = \frac{L}{2}\frac{Z_1(s)}{\sum_{n=0}^{\infty}\frac{Z_1(s)}{Z_1(s)+a_nZ_2(s)}}, \quad a_n = \frac{\pi^2(2n+1)^2}{4L^2} \quad (10)$$

Verification of impedance model and uncertainty estimation. In addition, to evaluate the values of electrical parameters from the proposed impedance model, the available published experimental results are used (Moeinkhah et al., 2013a). The nonlinear least square method is conducted to find the optimum parameters x^* that minimize the squared error between the experimental impedance response, $\hat{z}_i(i = 1, 2, \ldots, n)$ and our proposed theoretical model (Moeinkhah et al., 2013b). The identified parameters are listed in Table 1.

To characterize the proposed impedance model, the effect of different IPMC dimensions on impedance response is investigated. For this purpose, two samples with different dimensions were cut from one IPMC sheet and were labeled as big and short for referencing. Figure 3 compares the proposed impedance model with the experimental results for the short and big samples. As shown in Figure 3, the theoretical model closely follows the experimental results.

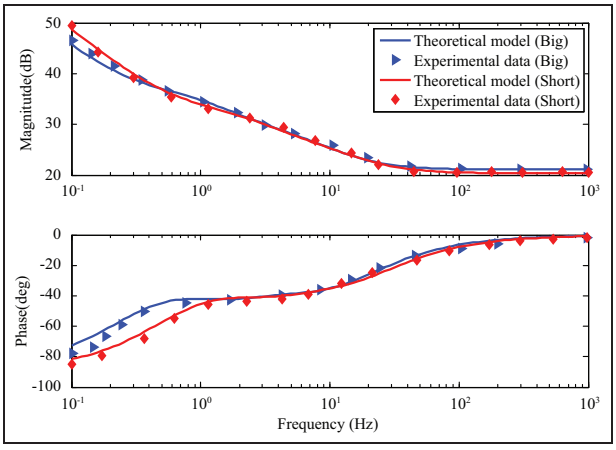

Figure 3. Comparison of the experimental impedance responses with the theoretical model.
Big: length = 37 mm, width = 5.5 mm, thickness = 360 μm.
Short: length = 25 mm, width = 5.5 mm, thickness = 360 μm.

To identify the finite-dimensional impedance model of the actuator, using the Golubev algorithm (Golubev and Horowitz, 1982; Moeinkhah et al., 2013b), different input signals (sin wave, step …) are applied to equation (9). Therefore, the uncertain impedance transfer function is obtained as

$$Z(s) = \frac{p_3s^3 + p_2s^2 + p_1s + p_0}{s^3 + q_2s^2 + q_1s + q_0} \quad (11)$$

where

$p_0 \in [213.5815,\ 248.7846]$; $p_1 \in [739.3541,\ 838.4842]$
$p_2 \in [267.4972,\ 298.1199]$; $p_3 \in [11.1817,\ 23.7714]$
$q_0 \in [0.006,\ 0.0073]$; $q_1 \in [9.0698,\ 11.0014]$;
$q_2 \in [7.7261,\ 9.5102]$

Figure 4 depicts the impedance Bode plot of the system with uncertainty and estimated impedance model. According to Figure 4, a family of third-order linear time invariant (LTI) system can predict the impedance model of the actuator in its operating frequency range.

Electromechanical model

This section focuses on the development of an analytical model to predict the deformation of an IPMC

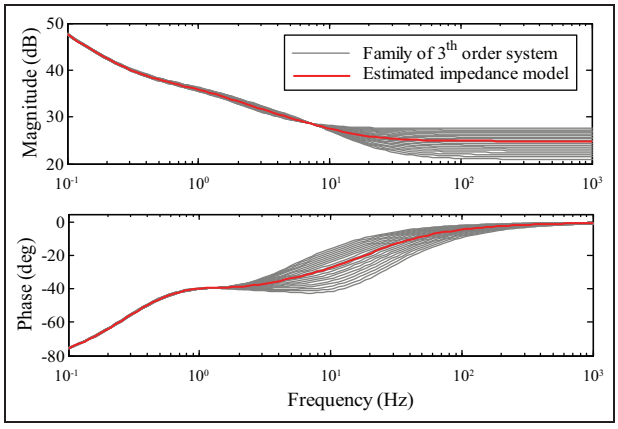

Figure 4. Impedance Bode plot of a family of third-order system and estimated model.

actuator subjected to an electric field. Under an electric field, cations are redistributed. Therefore, the imbalanced net charge density produces induced stress acting on the backbone polymer. It is experimentally shown (Nemat-Nasser and Li, 2000) that the induced stress is proportional to the charge density as

$$\sigma_i(x,s) = \alpha\rho(x,s) \tag{12}$$

where α is the coupling constant and $\rho(x,\ s)$ is the charge density as

$$\rho(x,t) = \frac{1}{Wh}\int_0^t \frac{i(x,t) - i(x+\mathrm{d}x,t)}{dx}\mathrm{d}t \tag{13}$$

where W and h are width and thickness of the actuator, respectively. This can be transformed into the Laplace domain, as

$$\begin{aligned}\rho(x,s) &= \frac{1}{Wh}\frac{1}{s}\left(-\frac{\partial i(x,s)}{\partial x}\right)\\ &= \frac{1}{sWh}\frac{V_0(s)}{Z_2(s)}\left(\cosh\left(\sqrt{\frac{Z_1(s)}{Z_2(s)}}x\right) - \tanh\left(\sqrt{\frac{Z_1(s)}{Z_2(s)}}L\right)\sinh\left(\sqrt{\frac{Z_1(s)}{Z_2(s)}}x\right)\right)\\ &= \frac{1}{sWh}\frac{V_0(s)}{Z_2(s)}g(x),\ g(x) = \cosh\left(\sqrt{\frac{Z_1(s)}{Z_2(s)}}x\right) - \tanh\left(\sqrt{\frac{Z_1(s)}{Z_2(s)}}L\right)\sinh\left(\sqrt{\frac{Z_1(s)}{Z_2(s)}}x\right)\end{aligned} \tag{14}$$

Hamilton's principle is used to obtain the dynamic equations of the flexible IPMC beam. Considering the structural damping as a result of linear viscoelastic behavior of Nafion and viscous damping force of water, the governing equation of motion based on Euler–Bernoulli beam theory can be obtained by substituting the strain energy, kinetic energy, and virtual work into Hamilton's principle

$$\begin{aligned}EI\frac{\partial^4 w(x,t)}{\partial x^4} + EI\frac{\gamma}{\omega}\frac{\partial^5 w(x,t)}{\partial x^4\partial t} + c_\nu(\omega)\frac{\partial w(x,t)}{\partial t}\\ + \mu_\nu(\omega)\frac{\partial^2 w(x,t)}{\partial t^2} = f_{app}(x,t) = \frac{\partial^2 M_{app}(x,t)}{\partial x^2}\end{aligned} \tag{15}$$

where $w(x,\ t)$ is transverse displacement, I is the area moment of inertia, E is static Young's modulus, A is the cross-sectional area of the IPMC, γ is an empirically determined value. Additionally, $f_{app}(x,\ t)$ and $M_{app}(x,\ t)$ are the distributed force density and the actuation-induced bending moment along the length of the actuator, respectively. The parameter $\mu_\nu(\omega)$ contains the added mass, $m_\nu(\omega)$, due to effect of fluid on the IPMC. The parameter $c_\nu(\omega)$ is damping coefficient of the viscous fluid. The details of the parameters $\mu_\nu(\omega)$, $c_\nu(\omega)$, and $m_\nu(\omega)$ are presented in Moeinkhah et al. (2013a). Equation (15) is a nonhomogeneous partial differential equation which incorporates the IPMC actuation force. Consider the improved distributed electrical model, equation (9), and using equations (12) and (14), we can obtain the actuation-induced bending moment as

$$\begin{aligned}M_{\mathrm{app}} &= 2\int_0^h z\sigma W\,\mathrm{d}z = 2\ W\int_0^h \alpha\rho(x,s)z\,\mathrm{d}z\\ &= \alpha h\frac{V_0(s)}{sZ_2(s)}g(x,s)\end{aligned} \tag{16}$$

The distributed force along the length in the Laplace domain will be obtained as

$$f_{\mathrm{app}}(x,s) = \frac{\partial^2 M_{\mathrm{app}}(x,s)}{\partial x^2} = \alpha h\frac{Z_1(s)}{sZ_2{}^2(s)}V_0(s)g(x,s) \tag{17}$$

In order to solve equation (15), the following transformations are used to normalize the variables

$$\begin{aligned}&\eta = \frac{x}{L},\quad \tau = \frac{t}{t_0},\quad y = \frac{w}{L}\\ &t_0 = L^2\sqrt{\frac{\mu_\nu(\omega)}{EI}},\quad \tilde{\gamma} = \frac{\gamma}{\omega\, t_0},\quad \tilde{c} = \frac{c_\nu(\omega)L^4}{EI\, t_0},\\ &F = \frac{EI}{L^3},\quad \tilde{f}(\eta,\tau) = \frac{f_{app}(\eta,\tau)}{F}\end{aligned} \tag{18}$$

Therefore, the normalized equation and corresponding boundary conditions are obtained as follows

$$y^{IV} + \tilde{\gamma}\dot{y}^{IV} + \tilde{c}\dot{y} + \ddot{y} = \tilde{f}(\eta, \tau) \tag{19}$$

$$\begin{aligned} y(0,\tau) = 0,\ \ y'(0,\tau) = 0 \\ y''(1,\tau) = 0,\ \ y'''(1,\tau) = 0 \end{aligned} \tag{20}$$

The primes and dots superscript used in equation (19) denote derivatives with respect to η and τ, respectively. According to the mode superposition principle, we can discrete the partial differential equation (19) into a set of ordinary differential equations. The flexural deflection of the cantilever beam can be estimated by using the assumed modes (Meirovitch, 1986)

$$y(\eta, \tau) = \sum_{i=1}^{n} \varphi_i(\eta) q_i(\tau) \tag{21}$$

where φ_i is the normal mode corresponding to the natural frequency ω_i and q_i is the corresponding generalized coordinate. Using the separation of variable method, the following eigenfunctions are obtained

$$\begin{aligned} \varphi_i(\eta) &= \cosh(\beta_i\eta) - \cos(\beta_i\eta) - \lambda_i(\sinh(\beta_i\eta) - \sin(\beta_i\eta)) \\ \lambda_i &= \frac{\sinh(\beta_i\eta) - \sin(\beta_i\eta)}{\cosh(\beta_i\eta) + \cos(\beta_i\eta)} \end{aligned} \tag{22}$$

where the eigenvalues β_i can be obtained based on the following characteristic equation

$$1 + \cosh(\beta_i)\cos(\beta_i) = 0 \tag{23}$$

By applying the orthogonal conditions of the normal modes, the uncoupled ordinary differential equations for the generalized coordinates, $q_i(s)$, can be obtained as

$$\ddot{q}_i(\tau) + \left(\tilde{\gamma}\omega_i^2 + \tilde{c}\right)\dot{q}_i(\tau) + \omega_i^2 q_i(\tau) = f_i(\tau) \quad i = 1, 2, \ldots, n \tag{24}$$

where

$$f_i(\tau) = \frac{1}{M_i}\int_0^1 \tilde{f}(\eta, \tau)\varphi_i(\eta)\mathrm{d}\eta,\ \ M_i = \int_0^1 \varphi_i^2(\eta)\mathrm{d}\eta \tag{25}$$

Upon transferring equation (25) into Laplace domain and integrating it, results can be simplified as

$$\begin{aligned} f_i(s) &= \Pi_i(s)V_0(s) \\ \Pi_i(s) &= \frac{\alpha h Z_1(s)}{sM_i F Z_2{}^2(s)}(1-b) \\ &[a_1 + b_1 - c_1 - d_1 - \lambda_i(a_1 - b_1 + \mathrm{j}c_1 - \mathrm{j}d_1)] \end{aligned} \tag{26}$$

where

$$\begin{aligned} a_1 &= \frac{\sinh(a+\beta_i)}{a+\beta_i},\ \ b_1 = \frac{\sinh(a-\beta_i)}{a-\beta_i}, \\ c_1 &= \frac{\sinh(a+\mathrm{j}\beta_i)}{a+\mathrm{j}\beta_i}, d_1 = \frac{\sinh(a-\mathrm{j}\beta_i)(L)}{a-\mathrm{j}\beta_i} \\ a &= \sqrt{\frac{Z_1(s)}{Z_2(s)}},\ \ b = \tanh\left(\sqrt{\frac{Z_1(s)}{Z_2(s)}}\right) \end{aligned} \tag{27}$$

Equation (24) shows that the dynamic response of an IPMC bending actuator can be modeled with n coupled ordinary differential equations. By substituting equation (22) and Laplace transform of equation (24) into equation (21), the transfer function $P(s)$ can be obtained as follows

$$P(s) = \frac{y(1,s)}{V_0(s)} = \sum_{i=1}^{n} \varphi_i(1)\left[s^2 + \left(\tilde{\gamma}\omega_i^2 + \tilde{c}\right)s + \omega_i^2\right]^{-1}\Pi_i(s) \tag{28}$$

Verification of the actuation model. In order to validate the proposed dynamic model, the available published experimental results are employed. This is done based on the experimental data of an IPMC strip having a 6 mm width, 37 mm length, and 0.22 mm thickness. The frequency response function (FRFs) based on small-oscillation theory is measured through a swept-sine method by applying sinusoidal actuation signal $V(t)$ with amplitude of 0.5 V and frequency from 0.1 to 20 Hz. To obtain the first natural frequency and damping ratio, the experimental result from a passive vibration test of an IPMC strip in water is used (Moeinkhah et al., 2013a). The remaining parameters, α and γ, are determined by minimizing the squared error between the empirical frequency response and the transfer function $P(s)$, equation (28). To do this, MATLAB function *lsqcurvefit*, which is usually used for nonlinear curve fitting, is employed. Table 2 shows all the parameters related to the beam dynamics.

To evaluate our proposed dynamic model, simulation results in both time and frequency domain are presented. Figure 5 compares the frequency response of the actuator with the experimental results. As illustrated in Figure 5, it is evident that the proposed model can predict the frequency-domain behavior of the actuator with good accuracy.

Table 2. Estimated values of the necessary dynamic parameters.

E (MPa)	ξ_1	μ_v (kg/m)	γ	α (J/C)
313	0.18	0.02	0.14	0.105

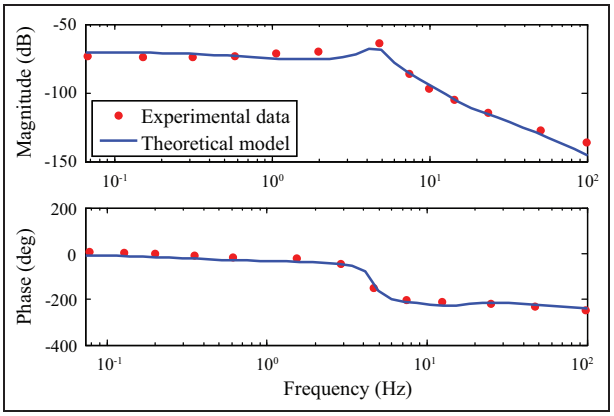

Figure 5. Comparison proposed an analytical frequency response with experimental results.

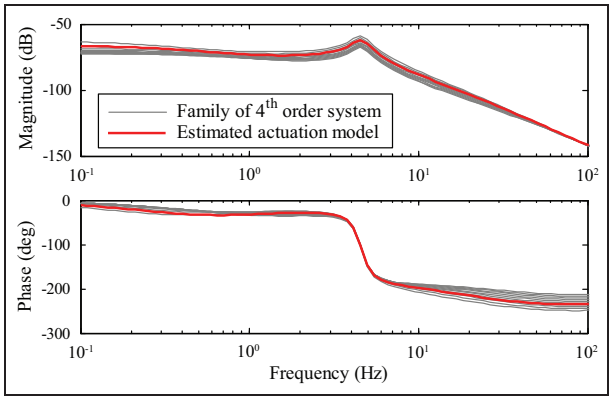

Figure 6. Bode plot of a family of the fourth-order actuation system and the estimated model.

Estimation of model uncertainty. An important motivation for developing a transfer function of an IPMC actuator is its potential use for real-time control. The driven actuation model, equation (28), is infinite-dimensional systems as it contains the terms "tanh(•)" and "sinh(•)." This model is not suitable for real-time control purpose. Therefore, the Golubev method will be used to build the finite-dimensional transfer function. As results, a family of the fourth-order LTI model is obtained as

$$P(s) = \frac{p_2 s^2 + p_1 s + p_0}{s^4 + q_3 s^3 + q_2 s^2 + q_1 s + q_0} \tag{29}$$

where

$$p_0 \in [0.0527,\ 0.1582];\ p_1 = 0.0774;$$
$$p_2 \in \left[1.647 \times 10^{-4},\ 4.941 \times 10^{-4}\right]$$
$$q_0 \in [73.5376,\ 661.8387];\ q_1 \in \left[335.6968,\ 1.0263 \times 10^{3}\right]$$
$$q_2 \in [39.0918,\ 95.8073];\ q_3 \in [16.6336,\ 48.0608]$$

Figure 6 shows Bode plot of the system response with uncertainty and the estimated actuation model. According to Figure 6, a family of the fourth-order LTI system can predict the actuation response of the IPMC actuator in its operating frequency range. This uncertain model will be used in the next section to design the QFT controller.

QFT control strategy

In spite of the positive characteristics of the IPMC actuators, they have some shortcomings such as hysteresis, back relaxation, low blocking force, and highly uncertain and nonlinear dynamics. These features cause challenges for modeling and design of a feedback controller for IPMC actuators and make it difficult to achieve suitable stability margins and good performance. To overcome these difficulties and to fulfill the performance specifications in the presence of uncertainties, robust control techniques are introduced. The objective of this section is to design a robust QFT controller for an IPMC bending actuator, which is represented by the derived uncertain transfer functions, equation (29).

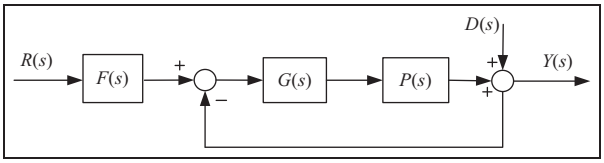

Figure 7. A two-degree-of-freedom feedback system.

QFT overview

QFT is a robust frequency-domain control design technique which offers direct insight into the available trade-off between controller complexity and performance specifications (Horowitz, 1992). System performance is commonly described as robust toward system instabilities, input or output disturbance rejection, and reference tracking. These requirements are represented as frequency constraints on the Nichols chart (NC). These constraints, as curves on the NC, are called QFT bounds. One of the main objectives in QFT procedure is to design a simple low-order controller with minimum bandwidth so as to avoid problems with noise amplification, resonances, and unmodeled high-frequency dynamics. Consider a two-degree-of-freedom feedback control system as shown in Figure 7. In Figure 7, $G(s)$ is a compensator, $F(s)$ is a pre-filter, and $D(s)$ is the disturbance at the plant output. $P(s)$ is an uncertain plant that belongs to a set of

$$\begin{aligned} &P(s) \in \{P(s,\alpha);\quad \alpha \in \Theta\}, \\ &\Theta = \left\{\alpha_i : \alpha_i \in \left[\alpha_i^{\min}, \alpha_i^{\max}\right],\quad i = 1, 2, \ldots, q\right\} \end{aligned} \tag{30}$$

where Θ is the vector of uncertain parameters.

In parametric uncertain systems, the plant templates, a set of points $P(jw_i)$ in the complex plane at specific frequencies, are generated prior to the QFT design. Given the plant templates, QFT converts closed-loop magnitude specifications into magnitude and phase constraints on a nominal open-loop function. The nominal open-loop transfer function, $L_0(s)$, is shaped so that the stability, tracking as well as disturbance boundaries on the NC are all satisfied. Consequently, the desired performance specifications are met. After loop-shaping process, the controller $G(s)$ is designed such that the system output, $y(t)$, lie within allowable tolerances. The resulting system has little sensitivity to parameters uncertainty and input–output disturbance during the process. If the control strategy is to track desired reference input then the pre-filter $F(s)$ must be designed to achieve the desired tracking closed-loop performance.

Performance specifications

Using the open-loop transmission, $L(s) = G(s)P(s)$, a robust controller $G(s)$ and a pre-filter $F(s)$ are synthesized such that the closed-loop system is stable for all plants and the following three conditions are satisfied.

1. *Robust stability specification*. In order to achieve a robust stability, it is sufficient to design a feedback compensator such that the frequency response envelope of all possible open-loop transfer functions does not intersect the critical point q_c. This point is located at $(-1, 0)$ in complex plane or at $(-180, 0\ \text{dB})$ in NC. The stability margin can be specified in terms of a phase margin (PM), gain margin (GM), or the corresponding M_L contour on the NC. If any one of these three stability requirements is specified, the remaining two can be calculated as follows

$$\begin{aligned} \text{GM} &= 20\log 10\left(1 + \frac{1}{M_L}\right)\ (\text{dB}) \\ \text{PM} &= 2\sin^{-1}\left(\frac{1}{2M_L}\right)\ (\text{deg}) \end{aligned} \tag{31}$$

The M_L contour places an upper limit on the magnitude of the closed-loop frequency response and forms a boundary which must not be intersected by a plot of the open-loop transmission. In this study, the desired stability margin for the closed-loop system has a reasonable range as follows

$$\left|\frac{L(j\omega)}{1 + L(j\omega)}\right| \le M_L = 1.4 \quad \text{for all } P, \quad \omega \ge 0 \tag{32}$$

2. *Tracking specification for the reference input*. Suppose $T_L(j\omega)$ and $T_U(j\omega)$ are the required lower and upper bounds for the magnitude of the closed-loop system control ratio, respectively. Thus, the magnitude of the tracking specifications can be expressed as follows

$$\begin{aligned} &|\,T_L(j\omega)\,| \le \left|\frac{L(j\omega)}{1 + L(j\omega)}\right| \le |\,T_U(j\omega)\,|, \\ &\forall \omega \in [0, \infty) \end{aligned} \tag{33}$$

Assume the following desired performance specification: (a) settling time of equal to 1.5 s and (b) maximum percentage overshoot of less than or equal to 10% for all uncertain plants. After some iterations using SISO design Toolbox-MATLAB, the upper and lower bounds are chosen as

$$\begin{aligned} T_U(s) &= \frac{0.9984}{0.0016s^3 + 0.0504s^2 + 0.3s + 1} \\ T_L(s) &= \frac{1}{0.0008s^4 + 0.0268s^3 + 0.2004s^2 + 0.8s + 1} \end{aligned} \tag{34}$$

3. *Disturbance rejection at plant output*. For disturbance rejection at the plant output, a sensitive reduction process must be followed. In this article, a constant upper tolerance is considered on the sensitivity function as follows

$$\left|\frac{1}{1 + L(j\omega)}\right|_{\max} \le 1.2, \quad \omega \ge 0 \tag{35}$$

Design of QFT controller

The three specifications defined by equations (32), (33), and (35) are used to determine the robustness, tracking performance, and output disturbance rejection boundaries on the NC at each critical frequency, respectively. The desired open-loop transfer function, $L(j\omega)$, must lie on or just above the bounds at each frequency to satisfy the required performance. In the first step in QFT design, a critical frequency array must be chosen for computing templates and bounds. Figure 8 shows a few critical bounds of the plant templates. As can be seen, for the uncertain plant set, equation (30), the templates are very similar in shape at frequencies higher than 1000 rad/s. Therefore, higher frequency bounds are not considered. As a result, the design frequencies are selected as $\omega = [0.2, 0.5, 1, 3, 4, 5, 10, 20, 100, 500, 1000]$ rad/s.

For loop shaping, the nominal loop has to satisfy the worst case of all bounds. Therefore, the loop shaping, or designing $G(s)$, involves changing the gain and adding poles and zeros until the nominal loop, $L_0(jw)$, lies within the specification bounds. To remove the steady-state error for the step reference input, the

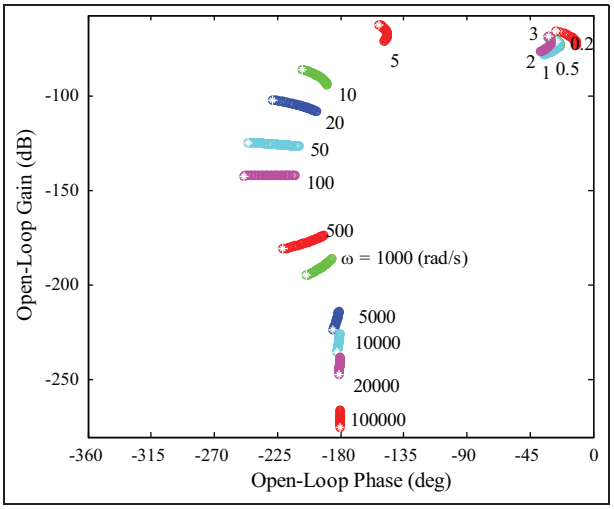

Figure 8. The boundary of the plant templates.

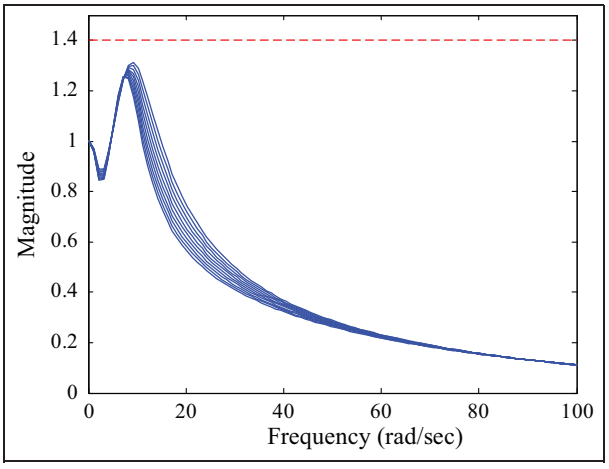

Figure 10. Magnitude of a family of transfer function $L(jw)/(1 + L(jw))$, equation (32).

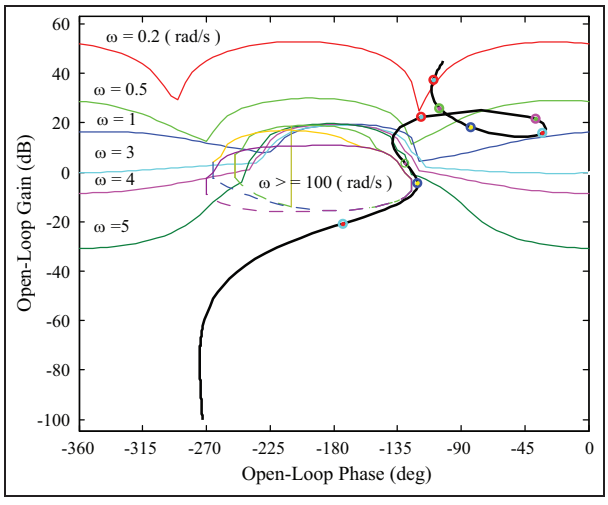

Figure 9. QFT bounds and loop shaping of $L(s)$ on the NC.
QFT: quantitative feedback theory; NC: Nichols chart.

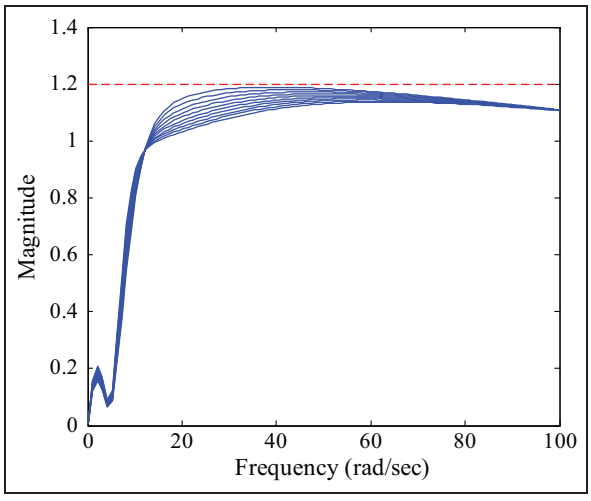

Figure 11. Magnitude of a family of transfer function $1/(1 + L(jw))$, equation (35).

compensator should have at least one integrator. Figure 9 shows QFT bounds and final loop shaping of the IPMC actuator.

Based on the above analysis, the robust controller $G(s)$ is given by

$$G(s) = 2.87 \times 10^4 \frac{(s/13.33 + 1)(s/3.7 + 1)(s/3.53 + 1)}{s(s/152 + 1)(s^2/150^2 + 1.4086\, s/150 + 1)} \quad (36)$$

To satisfy the tracking specification, a pre-filter is required to place the closed-loop frequency response between the lower and upper tracking bounds. The design of the pre-filter involves obtaining the worst upper and lower closed-loop responses of $L_0(s)F(s)/(1 + L_0(s))$ over the plant uncertainty. The peak value of the closed-loop Bode plot should be less than 0 dB in order to remove the overshoot of the step response. Consequently, the pre-filter is found as

$$F(s) = \frac{(s/147.3 + 1)}{s^2/3.53^2 + 1.3\, s/3.53 + 1} \quad (37)$$

Simulation of design

In this section, the effect of the designed QFT controller on the IPMC actuator is demonstrated using several numerical simulations. First, it must be ensured that the proposed controllers $G(s)$ and $F(s)$ satisfy the robust and tracking performances of the actuator. To validate $G(s)$, the design requirements (32) and (35) are checked using a family of uncertain transfer function $P(s)$. The magnitude of requirements (32) and (35) are shown in Figures 10 and 11, respectively. As shown in these

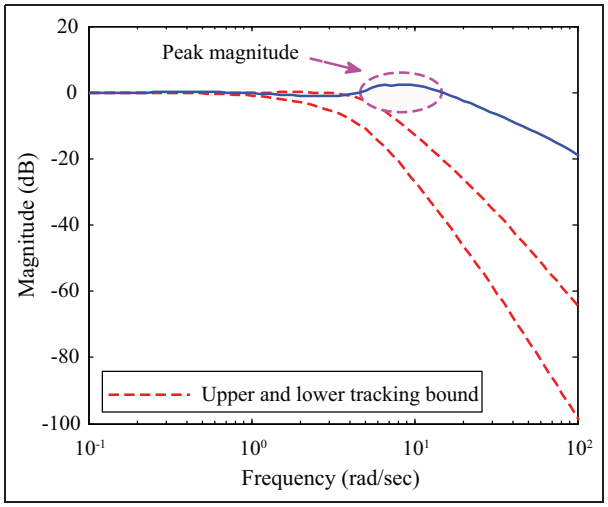

Figure 12. The closed-loop frequency response of the uncertain plant with the upper and lower tracking bounds without pre-filter.

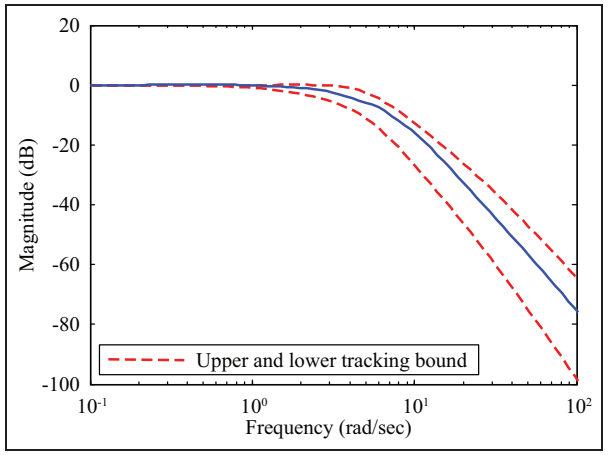

Figure 13. The closed-loop frequency response of the uncertain plant with the upper and lower tracking bounds with pre-filter.

figures, using the proposed controller $G(s)$, equation (36), the design requirements (32) and (35) are satisfied.

To validate $F(s)$, the tracking performance of the closed-loop system must be checked. The tracking specification of the closed-loop transfer function without pre-filter is shown in Figure 12. Clearly, the frequency response of the IPMC actuator violates the imposed tracking bounds, $T_L(j\omega)$ and $T_U(j\omega)$. As illustrated in Figure 12, the peak magnitude of the closed-loop is greater than 0 dB; therefore, the overshoot is expected for the step input.

To improve the time response for the reference input, a pre-filter is synthesized with two complex poles and one simple zero as demonstrated in equation (37). The effect of adding the pre-filter, $F(s)$, in the closed-loop frequency response is demonstrated in Figure 13. It is

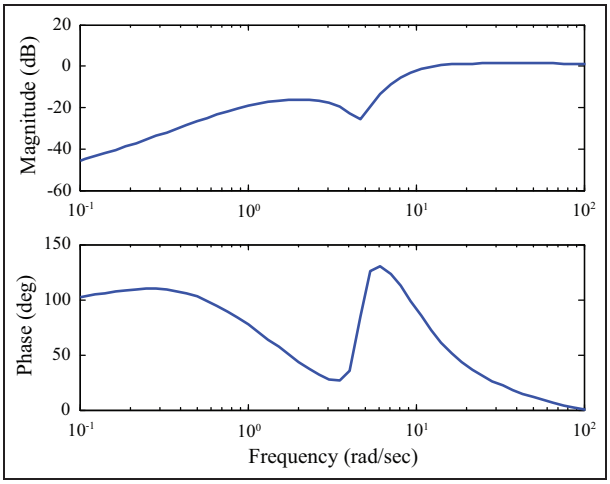

Figure 14. Bode plot of sensitivity function, $S(j\omega)$.

evident that the peak magnitude and the system bandwidth are reduced and therefore the Bode plot does not violate the tracking bounds.

The Bode plot of sensitivity function, $S(j\omega) = 1/(1 + L(j\omega))$, is shown in Figure 14. Since its magnitude is small in the low frequency range, then it can reject the external disturbances. In the high frequency range, the magnitude of $S(j\omega)$ is 0 dB which proves that it does not amplify the sensor noise.

Therefore, the designed QFT controller assures that the desired performance specifications, robust stability, output disturbance rejection, and reference tracking are all satisfied in the presence of plant uncertainty. Additionally, the performance of the designed QFT controller is compared with a traditional PID controller for several reference inputs. The simulation data of the tracking performance considering all uncertainties for a sinusoidal, square, and saw tooth input reference signals are presented in Figures 15 to 17. The comparison of these figures indicates that the QFT controller performs better than the PID controller for all three reference inputs.

Conclusion

This article investigated issues related to modeling, parameter identification, and robust control of an IPMC actuator. Unlike the previous study, where a maximum of second-order uncertain model was estimated for the IPMC actuator, this study considers the infinite-dimensional and nonlinear dynamics of the system and reduces it with a family of fourth-order transfer function. To do this, Hamilton's principle was used to obtain an exact electromechanical model to fully describe the dynamics of the IPMC actuators by considering structural damping, hydrodynamic loading, and electromechanical force. Utilizing the beam dynamics in viscous fluid, a nonhomogeneous partial

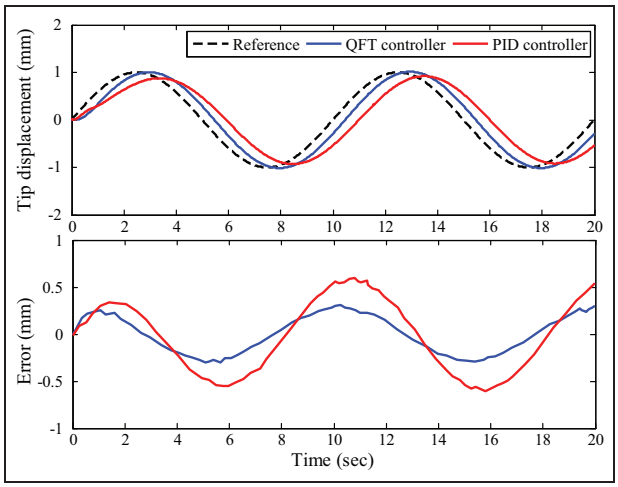

Figure 15. Tracking problem for all considered uncertainty under a sinusoidal reference input.
QFT: quantitative feedback theory; PID: proportional–integral–derivative.

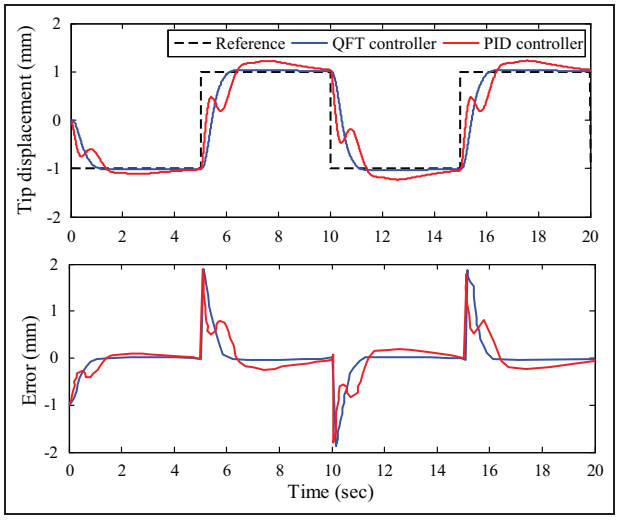

Figure 16. Tracking problem for all considered uncertainty under a square reference input.
QFT: quantitative feedback theory; PID: proportional–integral–derivative.

differential equation was developed for predicting the dynamic response of the actuator. Mode superposition principle was used for solving the dynamics equation of motion. The infinite-dimensional model was reduced to a family of fourth-order uncertain LTI system, using the Golubev method. The proposed dynamic model was validated based on published experimental data.QFT technique was next applied to the derived uncertain model of the IPMC actuator.

A strictly proper pre-filter transfer function and controller ($F(s)$, $G(s)$) were designed to satisfy the required specifications of having robust stability, robust tracking, and noise attenuation. Simulation of design indicates that the actuator has a satisfactory and consistent performance for both tracking and disturbance

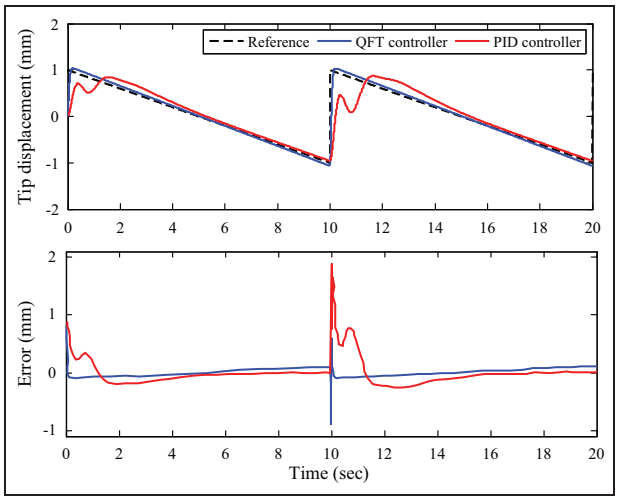

Figure 17. Tracking problem for all considered uncertainty under a saw tooth reference input.
QFT: quantitative feedback theory; PID: proportional–integral–derivative.

rejection problems. Additionally, the performance of the QFT controller was compared with a traditional PID controller. It was shown that the proposed controller has better tracking performance than the PID controller for several reference inputs, sinusoidal, square and saw tooth signals.

The main contribution of this article is (1) successfully applying the QFT technique to the IPMC actuator using the derived analytical fourth-order dynamic model. Additional contributions include (2) presenting an improved distributed RC model to better investigate electrical behavior at the interface between the polymer and the metal electrodes, (3) deriving an exact dynamic model for the IPMC actuator based on the Hamiltonian principle, and (4) replacing infinite-dimensional impedance and actuation model of IPMC actuator with a family LTI system based on the Golubev method.

Acknowledgements

The authors would like to express their thanks to Professor IL-Kwon Oh for providing helpful comments and access to his laboratory (Structural Dynamics & Smart Systems (SDSS) Lab, KAIST, South Korea) during the first author's sabbatical.

Declaration of conflicting interests

The authors declared no potential conflicts of interest with respect to the research, authorship, and/or publication of this article.

Funding

This research received no specific grant from any funding agency in public, commercial, or not-for-profit sectors.

References

Ahn KK, Truong DQ, Nam DNC, et al. (2010) Position control of ionic polymer metal composite actuator using quantitative feedback theory. *Sensors and Actuators A: Physical* 159(2): 204–212.

Bandopadhya D, Bhattacharya B and Dutta A (2008) Active vibration control strategy for a single-link flexible manipulator using ionic polymer metal composite. *Journal of Intelligent Material Systems and Structures* 19: 487–496.

Bao X, Bar-Cohen Y and Lih SS (2002) Measurements and macro models of ionomeric polymer-metal composites (IMPC). In: *Proceedings of SPIE: EAPAD conference*, San Diego, CA, 18–21 March, vol. 4695, pp. 286–293. Bellingham, WA: SPIE.

Bar-Cohen Y (2004) *Electroactive Polymer (EAP) Actuators as Artificial Muscles: Reality, Potential, and Challenges*. Bellingham, WA: SPIE.

Bar-Cohen Y and Zhang Q (2008) Electroactive polymer actuators and sensors. *MRS Bulletin* 33: 173–181.

Bhat N and Kim W (2003) System identification and control of ionic polymer metal composite. In: *Proceedings of SPIE: smart structures and materials*, San Diego, CA, 2 March, vol. 5049, pp. 526–535. Bellingham, WA: SPIE.

Bhat N and Kim W (2004a) Precision force and position control of an ionic polymer metal composite. *Proceedings of the Institution of Mechanical Engineers, Part I: Journal of Systems and Control Engineering* 218: 421–432.

Bhat ND and Kim W (2004b) Precision position control of ionic polymer metal composite. In: *Proceedings of the American control conference*, Boston, MA, 30 June–2 July, vol. 1, pp. 740–745. New York: IEEE.

Bonomo C, Fortuna L, Giannone P, et al. (2007) A nonlinear model for ionic polymer metal composites as actuators. *Smart Materials and Structures* 16(1): 1–12.

Branco PJC and Dente J (2006) Derivation of a continuum model and its electric equivalent-circuit representation for ionic polymer-metal composite (IPMC) electromechanics. *Smart Materials and Structures* 15(2): 378–392.

Brufau-Penella J, Tsiakmakis K, Laopoulos T, et al. (2008) Model reference adaptive control for an ionic polymer metal composite in underwater applications. *Smart Materials and Structures* 17(4): 045020.

Chen X, Zhu G, Yang X, et al. (2013) Model-based estimation of flow characteristics using an ionic polymer-metal composite beam. *IEEE/ASME Transactions on Mechatronics* 18(3): 932–943.

Chen Z and Tan X (2008) A control-oriented and physics-based model for ionic polymer-metal composite actuators. *IEEE/ASME Transactions on Mechatronics* 13(5): 519–529.

Chen Z, Shatara S and Tan X (2010) Modeling of biomimetic robotic fish propelled by an ionic polymer-metal composite caudal fin. *IEEE/ASME Transactions on Mechatronics* 15(3): 448–459.

Chen Z, Tan X, Will A, et al. (2007) A dynamic model for ionic polymer—metal composite sensors. *Smart Materials and Structures* 16(4): 1477–1488.

Feng GH and Tsai JW (2011) Micromachined optical fiber enclosed 4-electrode IPMC actuator with multidirectional control ability for biomedical application. *Biomedical Microdevices* 13(1): 169–177.

Golubev B and Horowitz I (1982) Plant rational transfer approximation from input-output data. *International Journal of Control* 36(4): 711–723.

Guo S, Fukuda T and Asaka K (2003) A new type of fish-like underwater microrobot. *IEEE/ASME Transactions on Mechatronics* 8(1): 136–141.

Horowitz IM (1992) *Quantitative Feedback Design Theory (QFT)*, vol. 1. Boulder, CO: QFT Publications.

Jeon JH, Kang SP, Lee S, et al. (2009) Novel biomimetic actuator based on SPEEK and PVDF. *Sensors and Actuators B: Chemical* 143(1): 357–364.

Jo C, Pugal D, Oh I-K, et al. (2013) Recent advances in ionic polymer-metal composite actuators and their modeling and applications. *Progress in Polymer Science* 38(7): 1037–1066.

Jung J-H, Vadahanambi S and Oh I-K (2010) Electro-active nano-composite actuator based on fullerene-reinforced Nafion. *Composites Science and Technology* 70(4): 584–592.

Kang S, Shin J, Kim SJ, et al. (2007) Robust control of ionic polymer-metal composites. *Smart Materials and Structures* 16(6): 2457–2463.

Kanno R, Tadokoro S, Takamori T, et al. (1996) Linear approximate dynamic model of an ICPF actuator. In: *Proceedings of IEEE international conference on robotics and automation*, Minneapolis, MN, 22–28 April, vol. 1, pp. 219–225. New York: IEEE.

Khadivi H, Aghazadeh B and Lucas C (2007) Fuzzy control of ionic polymer-metal composites. In: *29th annual international conference of the IEEE engineering in medicine and biology society*, Lyon, 23–26 August, pp. 4198–4201. New York: IEEE.

Kim B, Ryu J, Jeong Y, et al. (2003) A ciliary based 8-legged walking micro robot using cast IPMC actuators. In: *Proceedings of IEEE international conference on robotics and automation*, Taipei, Taiwan, 14–15 September, vol. 3, pp. 2940–2945. New York: IEEE.

Kim D and Kim KJ (2007) Can we overcome the relaxation of ionic polymer-metal composites? In: *Proceeding of SPIE: Electroactive Polymer Actuators and Devices (EPAD)*, San Diego, CA, 18 March, vol. 6524, p. 65240A (11 pp.). Bellingham, WA: SPIE.

Kim K (2007) Ionic polymer-metal composite as a new actuator and transducer material. In: KJ Kim and S Tadokoro (eds) *Electroactive Polymers for Robotic Applications: Artificial Muscles and Sensors*. London: Springer-Verlag, pp. 153–164.

Kim KJ and Shahinpoor M (2003) Ionic polymer-metal composites. II. Manufacturing techniques. *Smart Materials and Structures* 12(1): 65–79.

La HM and Sheng W (2009) Robust adaptive control with leakage modification for a nonlinear model of ionic polymer metal composites (IPMC). In: *IEEE International Conference on Robotics and Biomimetics (ROBIO)*, Bangkok, Thailand, 22–25 February, pp. 1783–1788. New York: IEEE.

Lavu BC, Schoen MP and Mahajan A (2005) Adaptive intelligent control of ionic polymer-metal composites. *Smart Materials and Structures* 14(4): 466–474.

Liu D, McDaid A, Aw K, et al. (2011) Position control of an ionic polymer metal composite actuated rotary joint using iterative feedback tuning. *Mechatronics* 21(1): 315–328.

McDaid A, Aw K, Patel K, et al. (2010) Development of an ionic polymer-metal composite stepper motor using a novel actuator model. *International Journal of Smart and Nano Materials* 1(4): 261–277.

Mallavarapu K and Leo DJ (2001) Feedback control of the bending response of ionic polymer actuators. *Journal of Intelligent Material Systems and Structures* 12: 143–155.

Meirovitch L (1986) *Elements of Vibration Analysis*. New York: McGraw-Hill.

Moeinkhah H, Jung JY, Jeon J, et al. (2013a) How does clamping pressure influence actuation performance of soft ionic polymer-metal composites? *Smart Materials and Structures* 22(2): 025014 (11 pp.).

Moeinkhah H, Rezaeepazhand J and Akarzadeh A (2013b) analytical dynamic modeling of a cantilever IPMC actuator based on distributed electrical circuit. *Smart Materials and Structures* 22(5): 055033 (10 pp.).

Nemat-Nasser S and Li JY (2000) Electromechanical response of ionic polymer-metal composites. *Journal of Applied Physics* 87(7): 3321–3331.

Newbury KM and Leo DJ (2003) Linear electromechanical model of ionic polymer transducers—part I: model development. *Journal of Intelligent Material Systems and Structures* 14: 333–342.

Panda B and Dutta A (2010) Design of a partially compliant crank rocker mechanism using ionic polymer metal composite for path generation. *Materials & Design* 31(5): 2471–2477.

Porfiri M (2009) An electromechanical model for sensing and actuation of ionic polymer metal composites. *Smart Materials and Structures* 18(1): 015016 (16 pp.).

Pugal D, Kim KJ and Aabloo A (2011) An explicit physics-based model of ionic polymer-metal composite actuators. *Journal of Applied Physics* 110: 084904 (9 pp.).

Richardson RC, Levesley MC, Brown MD, et al. (2003) Control of ionic polymer metal composites. *IEEE/ASME Transactions on Mechatronics* 8(2): 245–253.

Santos J, Lopes B and Branco P (2010) Ionic polymer-metal composite material as a diaphragm for micropump devices. *Sensors and Actuators A: Physical* 161(1–2): 225–233.

Shahinpoor M and Kim KJ (2000) The effect of surface-electrode resistance on the performance of ionic polymer-metal composite (IPMC) artificial muscles. *Smart Materials and Structures* 9(4): 543–551.

Shahinpoor M and Kim KJ (2001) Ionic polymer-metal composites. I. Fundamentals. *Smart Materials and Structures* 10(4): 819–833.

Shahinpoor M and Kim KJ (2005) Ionic polymer-metal composites. IV. Industrial and medical applications. *Smart Materials and Structures* 14(1): 197–214.

Takagi K, Hirayama S, Sano S, et al. (2012) Reduction of the stress-relaxation of IPMC actuators by a fluctuating input and with a cooperative control. In: *Proceedings of SPIE: Electroactive Polymer Actuators and Devices (EAPAD)*, San Diego, CA, 11 March, vol. 8340, 83402J (8 pp). Bellingham, WA: SPIE.

Thinh NT, Yang YS and Oh IK (2009) Adaptive neuro-fuzzy control of ionic polymer metal composite actuators. *Smart Materials and Structures* 18(6): 065016 (12 pp.).

Yamakita M, Kamamichi N, Kozuki T, et al. (2005) A snake-like swimming robot using IPMC actuator and verification of doping effect. In: *IEEE/RSJ International Conference on Intelligent Robots and Systems (IROS)*, Edmonton, AB, Canada, 2–6 August, pp. 2035–2040. New York: IEEE.

Yeom SW and Oh IK (2009) A biomimetic jellyfish robot based on ionic polymer metal composite actuators. *Smart Materials and Structures* 18(8): 085002 (10 pp.).

Yim W, Lee J and Kim KJ (2007) An artificial muscle actuator for biomimetic underwater propulsors. *Bioinspiration & Biomimetics* 2(2): S31–S41.

Yousef H, Boukallel M and Althoefer K (2011) Tactile sensing for dexterous in-hand manipulation in robotics – a review. *Sensors and Actuators A: Physical* 167(2): 171–187.

Yun K and Kim W (2006) Microscale position control of an electroactive polymer using an anti-windup scheme. *Smart Materials and Structures* 15(4): 924–930.